

Light beam coupling between standard single mode fibers and highly nonlinear photonic crystal fibers based on the fused biconical tapering technique

Jianguo Liu,^{1,*} Tee-Hiang Cheng,¹ Senior Member, IEEE, Yong-kee Yeo,² Yixin Wang,² Lifang Xue,³ Member, OSA, Zhaowen Xu,¹ and Dawei Wang¹

¹ School of Electrical & Electronic Engineering, Nanyang Technological University, 639798, Singapore.

² Institute for Infocomm Research, 21 Heng Mui Keng Terrace, 11961,3 Singapore,

³ Semiconductor Institute of CAS, Beijing, 10083, China

*Corresponding author: jgliu@ntu.edu.sg

Abstract: We propose and experimentally demonstrate light beam coupling between a single-mode fiber (SMF) and a highly nonlinear photonic crystal fiber (HN-PCF) based on the fused biconical tapering (FBT) technique. In our experiment, a standard SMF is pre-tapered to match its propagation constant to that of a HN-PCF. In order to remove the condensation in the air holes, the temperature is increased gradually to preheat the fibers. An appropriate level of hydrogen flow is administered to avoid the air-hole collapse. As a result, coupling ratio exceeding 90% between the SMF and HN-PCF is achieved. This technique avoids back Fresnel reflection, mode-field diameter (MFD) mismatch and fiber-core misalignment, bubble generation and air-hole collapse in the interface fusion splice.

©2008 Optical Society of America

OCIS codes: (060.1810) Buffers, couplers, routers, switches, and multiplexers; (060.2310) Fiber Optics..

References and links

1. Philip Russell, "Photonic Crystal Fibers," *Science* **299**, 358-362 (2003).
2. J. C. Knight, T. A. Birks, P. Russell, and D. M. Atkin, "All-silica single-mode optical fiber with photonic crystal cladding," *Opt. Lett.* **21**, 1547-1549 (1996).
3. N. A. Mortensen, M. D. Nielsen, and J. R. Folkenberg, "Improved large-mode-area endlessly single-mode photonic crystal fibers," *Opt. Lett.* **28**, 393-395 (2003).
4. J. C. Knight, J. Arriaga, A. Ortigosa-Blanch, W. J. Wadsworth, and P. St. J. Russell, "Anomalous dispersion in photonic crystal fiber," *IEEE Photon. Technol. Lett.* **12**, 807-809 (2000).
5. A. Ferrando, E. Silvestre, P. Andrés, J. J. Miret, and M. V. Andrés, "Designing the properties of dispersion-flattened photonic crystal fibers," *Opt. Express* **9**, 687-697 (2001), <http://www.opticsinfobase.org/abstract.cfm?uri=oe-9-13-687>.
6. T. A. Birks, J. C. Knight, and P. S. J. Russell, "Endlessly single-mode photonic crystal fiber," *Opt. Lett.* **22**, 961-963 (1997).
7. K. Saitoh and M. Koshiba, "Highly nonlinear dispersion-flattened photonic crystal fibers for supercontinuum generation in a telecommunication window," *Opt. Express* **12**, 2027-2032 (2004), <http://www.opticsinfobase.org/abstract.cfm?uri=oe-12-10-2027>.
8. J. E. Sharping, M. Fiorentino, P. Kumar, and R. S. Windeler, "Optical parametric oscillator based on four-wave mixing in microstructure fiber," *Opt. Lett.* **27**, 1675-1677 (2002).
9. J. K. Ranka, R. S. Windeler, and A. J. Stentz, "Visible continuum generation in air-silica microstructure optical fibers with anomalous dispersion at 800 nm," *Opt. Lett.* **25**, 25-27 (2000).
10. P. Petropoulos, T. M. Monro, W. Belardi, K. Furusawa, J. H. Lee, and D. J. Richardson, "2R-regenerative all-optical switch based on a highly nonlinear holey fiber," *Opt. Lett.* **26**, 1233-1235 (2001).
11. J. E. Sharping, M. Fiorentino, P. Kumar, and R. S. Windeler, "All-optical switching based on cross-phase modulation in microstructure fiber," *IEEE Photon. Technol. Lett.* **14**, 77-79 (2002).
12. T. T. Larsen, J. Broeng, D. S. Hermann, and A. Bjarklev, "Thermo-optic switching in liquid crystal infiltrated photonic bandgap fibres," *Electron. Lett.* **39**, 1719-1720 (2003).

13. W. J. Wadsworth, J. C. Knight, W. H. Reeves, and P. St. J. Russell, "Yb³⁺-doped photonic crystal fibre laser," *Electron. Lett.* **36**, 1452-1454 (2000).
14. W. Wadsworth, R. Percival, G. Bouwmans, J. Knight, and P. Russell, "High power air-clad photonic crystal fibre laser," *Opt. Express* **11**, 48-53 (2003), <http://www.opticsexpress.org/abstract.cfm?uri=OE-11-1-48>.
15. Y. L. Hoo, W. Jin, H. L. Ho, D. N. Wang, and R. S. Windeler, "Evanescent-wave gas sensing using microstructure fiber," *Opt. Engin.* **41**, 8-9 (2002).
16. L. Zou, X. Bao, S. Afshar V., and L. Chen, "Dependence of the Brillouin frequency shift on strain and temperature in a photonic crystal fiber," *Opt. Lett.* **29**, 1485-1487 (2004).
17. T. Larsen, A. Bjarklev, D. Hermann, and J. Broeng, "Optical devices based on liquid crystal photonic bandgap fibres," *Opt. Express* **11**, 2589-2596 (2003), <http://www.opticsinfobase.org/abstract.cfm?uri=oe-11-20-2589>.
18. W. N. Macpherson, M. J. Gander, McBride, J. D. C. Jones, P. M. Blanchard, J. G. Burnett, A. H. Greenaway, B. Mangan, T. A. Birks, J. C. Knight, and P. St. J. Russell, "Remotely addressed optical fibre curvature sensor using multicore photonic crystal fibre," *Opt. Commun.* **193**, 97-104 (2001).
19. C. Zhang, G. Kai, Z. Wang, T. Sun, C. Wang, Y. Liu, W. Zhang, J. Liu, S. Yuan, and X. Dong, "Transformation of a transmission mechanism by filling the holes of normal silica-guiding microstructure fibers with nematic liquid crystal," *Opt. Lett.* **30**, 2372-2374 (2005).
20. Y. Zhu, P. Shum, H. -W. Bay, M. Yan, J. Hu, J. Hao, and C. Lu, "Strain-insensitive and high-temperature long-period gratings inscribed in photonic crystal fiber," *Opt. Lett.* **30**, 367-369 (2005).
21. B. Bourliaguet, C. Paré, F. Émond, A. Croteau, A. Proulx, and R. Vallée, "Microstructured fiber splicing," *Opt. Express* **11**, 3412-3417 (2003), <http://www.opticsexpress.org/abstract.cfm?uri=OE-11-25-3412>.
22. B. H. Park, J. Kim, U. C. Paek, and B. H. Lee, "The optimum fusion splicing conditions for a large mode area photonic crystal fiber," *IEICE Trans. Electron.* **E88-C**, 883-888 (2005).
23. A. D. Yablon, and R. T. Bise, "Low-loss high-strength microstructured fiber fusion splices using GRIN fiber lenses," *IEEE Photon. Technol. Lett.* **17**, 118-120 (2005).
24. R. Thapa, K. Knabe, K. L. Corwin, and B. R. Washburn, "Arc fusion splicing of hollow-core photonic bandgap fibers for gas-filled fiber cells," *Opt. Express* **14**, 9576-9583 (2006), <http://www.opticsexpress.org/abstract.cfm?uri=OE-14-21-9576>.
25. L. M. Xiao, W. Jin, and M. S. Demokan, "Fusion splicing small-core photonic crystal fibers and single-mode fibers by repeated arc discharges," *Opt. Lett.* **32**, 115-117 (2007).
26. J. C. Fajardo, M. T. Gallagher, and Q. Wu, "Splice joint and process for joining a microstructured optical fiber and a conventional optical fiber," U.S. Patent 20030081915A1 (2003).
27. O. Frazão, J. P. Carvalho, and H. M. Salgado, "Low-loss splice in a microstructured fibre using a conventional fusion splicer," *Microw. Opt. Technol. Lett.* **46**, 172-174 (2005).
28. H. Y. Tam, "Simple fusion splicing technique for reducing splicing loss between standard single mode fibres and erbium-doped fibre," *Electron. Lett.* **27**, 1597-1599 (1991).
29. J. H. Chong, M. K. Rao, Y. Zhu, and P. Shum, "An effective splicing method on photonic crystal fiber using CO₂ laser," *IEEE Photon. Technol. Lett.* **15**, 942-944 (2003).
30. J. H. Chong, and M. K. Rao, "Development of a system for laser splicing photonic crystal fiber," *Opt. Express* **11**, 1365-1370 (2003), <http://www.opticsexpress.org/abstract.cfm?uri=OE-11-12-1365>.
31. S. G. Leon-Saval, T. A. Birks, N. Y. Joly, A. K. George, W. J. Wadsworth, G. Kakarantzas, and P. St. J. Russell, "Splice-free interfacing of photonic crystal fibers," *Opt. Letters* **30**, 1629-1631 (2005).
32. Norbert Grote and Herbert Venghaus, *Fibre Optic Communication devices* ISBN 3-540-66977-9 (Springer-Verlag Berlin Heidelberg New York).
33. B. S. Kawasaki, K. O. Hill, and R. G. Lamont, "Biconical-taper single-mode fiber coupler," *Opt. Lett.* **327-328** (1981).
34. J. B. Eom, D.S. Moon, U. C. Paek, and B. H. Lee, "Fabrication and transmission characteristics of couplers using photonic crystal fibers," *OFC2002*, 465-466 (2002)
35. H. Kim, J. Kim, U.-C. Paek, and B. Ha Lee, "Tunable photonic crystal fiber coupler based on a side-polishing technique," *Opt. Lett.* **29**, 1194-1196 (2004)
36. L. Xiao, M. S. Demokan, W. Jin, Y. Wang, and C.-L. Zhao, "Fusion Splicing Photonic Crystal Fibers and Conventional Single-Mode Fibers: Microhole Collapse Effect," *J. Lightwave Technol.* **25**, 3563-3574 (2007).
37. J. Liu, G. Kai, L. Xue, Z. Wang, Y. Liu, Y. Li, C. Zhang, T. Sun, and X. Dong, "Modal cutoff properties in germanium-doped photonic crystal fiber," *Appl. Opt.* **45**, 2035-2038 (2006).

1. Introduction

Photonic crystal fibers (PCFs) have attracted a lot of researchers' interests due to such unique characters as endless single-mode transmission, flexible chromatic dispersion, large mode area, and high nonlinearity etc. [1-7]. Due to their flexible structures, PCFs have been used for a number of fiber-optic devices—such as optical switches, wavelength converters, high-power

fiber lasers, supercontinuum light sources, and gas sensors etc.—that are difficult to achieve using conventional fibers [7-20].

The main causes of splicing loss are mode-field mismatch, core axis misalignment, structure deformation, end face stuffing, and difference in softening temperature among different fibers types. The flexibility in the design of the air-hole array make the MFDs of PCFs vary from submicron to tens of microns. Furthermore, the softening temperature and thermal expansion coefficients are different due to the differing material structural design between PCFs and SMFs. Finally, the impurity that infiltrates into the air holes also changes the characteristics of the PCF. Therefore, a low loss interface splice between the SMF and PCF is very difficult to achieve. The large splicing loss restricts the applications of PCF based devices because it is very difficult to incorporate such lossy devices into standard communication or sensing systems.

Many researchers have investigated the splicing problem. The methods can be categorized into three types: (I) Electric arc splicing technique [21-28]; (II) Carbon dioxide (CO₂) laser heating splicing technique [29, 30]; (III) Splice-free interfacing of photonic crystal fibers [31]. For Type I, although many experiments have been done, it is still very difficult to solve the problem of MFD mismatch, air-hole collapse and bubbles growing during the fusion splicing process. For Type II, the major problem is that it is not easy to align SMF core to that of PCF with the later's complicated structure. For Type III, the undrawn end of ferrule makes PCF based devices very bulky and inflexible for many applications. Furthermore, for all the three types, Fresnel back-reflection at the splice interface and the Fabry-Perot (F-P) resonant cavity effect arising from the differences in properties of the two kinds of the fibers can cause system instability and in the worst case cause damage to the system. It is clear from the above discussion that low-loss splicing of a PCF to a conventional SMF is a very challenging problem to be solved.

Besides interface fusion splicing, coupling is another effective method for transferring the light power from one fiber to another. FBT technique is one of most widely methods used for fabricating couplers. In this technique, two fibers are placed side by side and thermally fused with hydrogen flame while being pulled until certain coupling ratio was achieved [32, 33]. Eom *et al.* [34] used the FBT technique to achieve coupling between PCFs with coupling ratios of 67/33 and 52/48. Hokyung Kim *et al.* [35] demonstrated evanescent field coupling between the core modes of two PCFs by using side polishing to bring the cores close to each other and they showed that by adjusting the mating angle between the two side-polished PCFs, 90% coupling ratio can be achieved.

In this paper, we describe a low loss method for transferring the power between a SMF and a HN-PCF without the need for interface splicing. A HN-PCF is twisted with a pre-tapered SMF before being tapered; the temperature is increased gradually to remove the condensation in the air holes till it reaches the working temperature. In our experiment, more than 90% coupling between a SMF to a HN-PCF is achieved. This method avoids the MFD mismatch problem, Fresnel back-reflection and fiber-core nonalignment that exist inherently in the interface splicing method.

2. Theory

Due to the flexibility in designing PCFs, the MFD of the PCFs are usually different from that of the standard SMF. As suggested in Ref. [36], when the interface fusion splicing technique is used to splice a PCF with a standard SMF, the splicing loss derived from the MFD mismatch can be expressed as,

$$\alpha = -20 \log \left(\frac{2\omega_{PCF}\omega_{SMF}}{\omega_{PCF}^2 + \omega_{SMF}^2} \right) \quad (1)$$

where $2\omega_{PCF}$ and $2\omega_{SMF}$ are the MFDs of the PCF and SMF, respectively. Besides the mismatch in MFDs, splicing loss also increases due to the presence of bubbles caused by air-hole collapse, which is caused by the difference in softening temperature between standard

SMF and PCF and the condensation in the air holes. How to resolve the aforementioned problems in the light beam coupling between SMF and PCF remains a key problem to be solved.

According to the Coupling Mode theory, when two parallel fibers are sufficiently close, an exchange of power takes place between the fibers in a periodic fashion along the direction of propagation. When all the light is input from the entrance of Fiber 1, the powers in the two fibers can be expressed as [32]

$$P_1 = P_0 \left(1 - \left| \frac{K_C}{\delta_{\text{eff}}} \right| \sin^2(\delta_{\text{eff}} z) \right) \quad (2)$$

$$P_2 = P_0 \left| \frac{K_C}{\delta_{\text{eff}}} \right|^2 \sin^2(\delta_{\text{eff}} z) \quad (3)$$

where P_0 , P_1 and P_2 are the input power, the power in Fiber 1 and the power in Fiber 2, respectively. $\delta_{\text{eff}} = \sqrt{(\beta_1 - \beta_2)^2 + |K_C|^2}$, where β_1 and β_2 are the propagation constant of Fiber 1 and Fiber 2, respectively. It can be seen from the equations that β_1 should be matched to β_2 so that the coupling ratio is high. It also can be seen from the equations that the coupling ratio will reach the maximum when $\delta_{\text{eff}} z = \pm (2n+1)\pi/2$, where n is an integer. K_C is the coupling coefficient, which is determined by the properties of the fibers and the space between the fiber cores. In order to enhance the coupling effect between the fibers, the cores of the fibers have to be close to each other.

We use the Beam Propagation Method to simulate the coupling between tapered waveguides. In Fig.1, the left figure is the model of the coupling between the tapered waveguides. The graph on the right shows that the normalized powers in the two waveguides vary along the tapering axis. It can be seen that coupling will occur when the waveguides are close to each other.

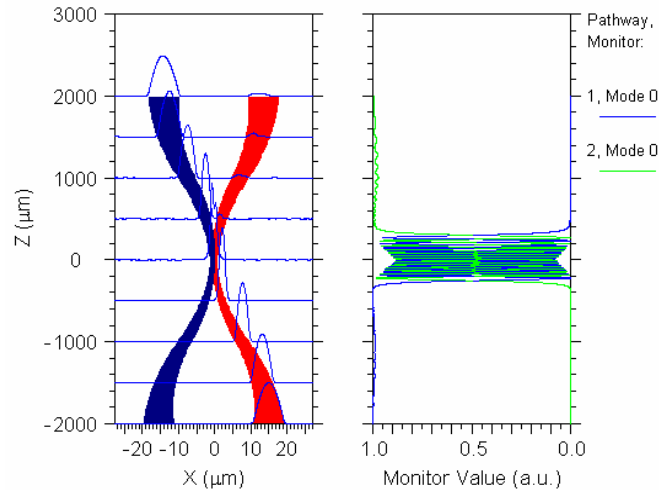


Fig.1. The model of coupling between tapered waveguides

3. Experiment

Figure 2 shows the experimental setup. H1 and H2 are fiber holders. After being stripped off their polymer coating, a SMF (black line) and a HN-PCF (red line) were put into the V-grooves and clamped after twisting. When the hydrogen flame torch is fired up, the fibers are heated up to their softening temperature then tapered and fused with the holders moving along

the orbit in opposite direction. Coupling occurs between the SMF and the HN-PCF when their cores move so close that their mode fields overlap. LD is a laser diode with a center wavelength of 1550nm. PD1 and PD2 are power detectors. C is a computer, which is used to control H1, H2, PD1 and PD2.

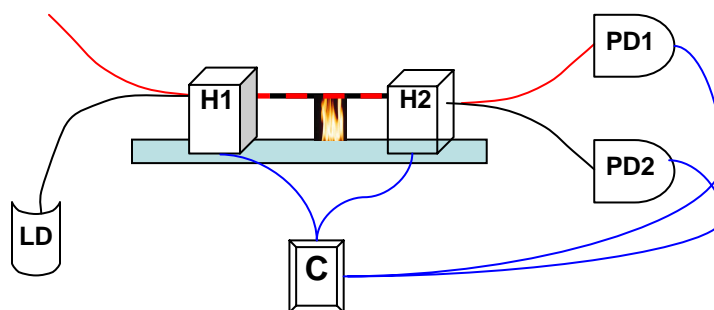


Fig. 2. The experimental setup

Table 1. The parameters of the coupler station

Value	Parameter Name
60.000002	Drawing speed (60-300um/sec)
21.300000	Package Forward (0-22.5mm)
6.100000	Package Height (0-7.5mm)
2.000000	Pre-Heating Time (sec)
40.000000	Fiber Holder Spacing, Standard (35-55mm)
40.000000	Fiber Holder Spacing, Wideband (35-55mm)
2.000000	Torch Height, Standard (0-12.7mm)
0.999000	Stop Coupling Ratio, Std (0.001-0.999)
5.000000	Pre-Draw Length (0.001-20.0mm)
2.000000	Number of Fibers
55.000000	Hydrogen flow (A.U.)

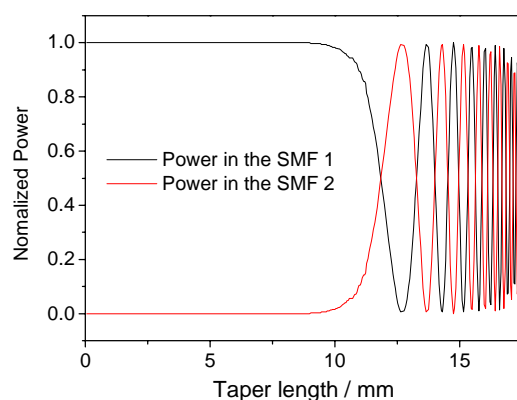


Fig. 3. Power conversion in the SMFs with the taper length increasing.

Firstly, coupling between SMFs is done in order to test the performance of the experiment setup. Table 1 shows the experimental parameters. Figure 3 shows the power conversions in the SMFs with the taper length increasing. It can be seen that coupling takes place when the taper length is almost 9.5mm, and almost all the power is transferred into SMF 2 from SMF 1 when the taper length is 12.8mm. Moreover, the period of coupling declines with the taper length increasing, which results from the substantial increase in coupling coefficient when the taper becomes thinner. The results are in good agreement with Eq. (2) and (3).

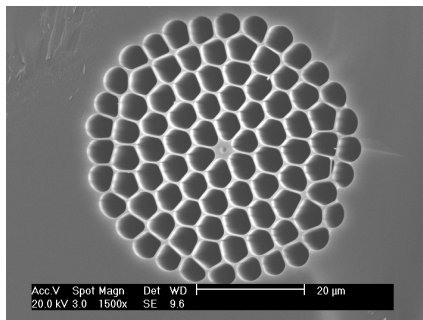


Fig.4. The Transverse section of the HN-PCF

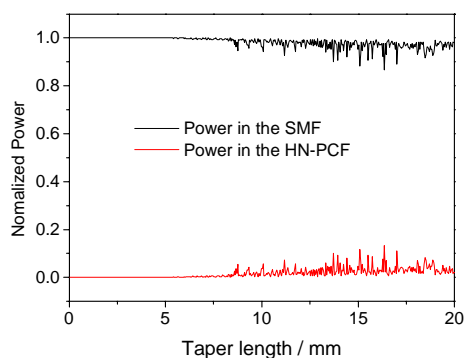


Fig. 5. The coupling result of the SMF to the HN-PCF directly with the parameter as shown in Table 1.

In our experiment, a HN-PCF fabricated by Yangtze Optical Fiber and Cable Company LTD. (YOFC) (Code: APR00042DB0) is used to splice with an SMF. The cross section of the HN-PCF is shown in Fig. 4. It can be seen that the core diameter of the HN-PCF is far less than that of SMF. In our experiment, the highest coupling efficiency achieved with direct splicing technique is less than 0.113, which is very low. Fig.5 shows the coupling result of an SMF coupled directly to the HN-PCF with the parameters shown in Tale 1. It can be seen that coupling starts at a taper length of about 8mm, but the maximum achievable coupling ratio is only about 10%. The low coupling ratio is partly due to the mismatch in propagation constants of the two fibers and partly due to air hole collapses.

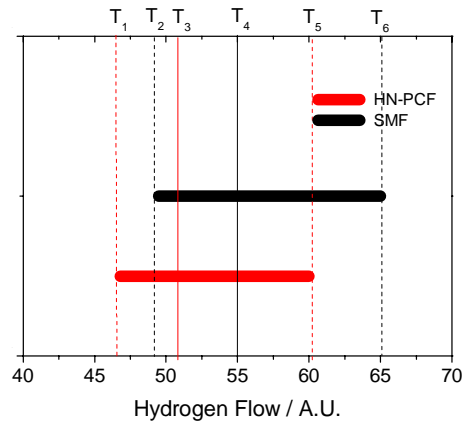


Fig. 6. The melting process schematic of the HN-PCF and the SMF

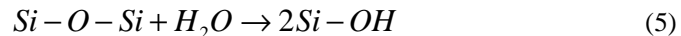
In the tapering process, the twisted fibers are heated above the softening temperature and melted together to achieve the power coupling. For a PCF, the rate of air hole collapse is given by [36],

$$V_{collapse} = \frac{\gamma}{2\eta} \quad (4)$$

where γ is the surface tension and η is the viscosity. The viscosity, which is a function of temperature, is the most important property of silica glass and affects its structural formation. When the temperature of heated PCFs exceeds the softening point by a great deal, the surface tension will overcome the viscosity and cause the PCF's cylindrical air holes to collapse. Furthermore, the softening point of the PCFs is lower than that of SMFs because PCFs have a smaller average solid silica diameter (due to air-silica structures) than that of conventional SMFs [30]. Assuming that the heat absorption coefficient is almost the same for PCFs and SMFs, the surface tension of silica is not very sensitive to temperature over the range encountered in tapering, but the viscosity of silica sharply decreases with increasing temperature, so the rate of air hole collapses increases with temperature. Therefore, the PCF needs a lower temperature to melt the fiber if the absorption coefficient is almost constant for both fibers.

Figure 6 shows the melting process schematic of the HN-PCF and SMF with the hydrogen flow. It can be seen that the HN-PCF starts to soften at temperature T1, which is lower than that of SMF T2; and the HN-PCF will melt to liquid at temperature T5, which is also lower than that of SMF T6. For the SMF taper we choose temperature T4. In order to avoid air hole collapse, we have to reduce the hydrogen flow to accommodate the different optical properties of the two fibers. The hydrogen flow used is sufficiently low so as not to damage the HN-PCF but higher than T2 so that the SMF can be softened, in other words, the heat temperature is lower than T4 but higher than T2, such as T3.

Moreover, the optical fiber material consists of silicon (Si) and oxygen (O). Any composition introduced in the fiber will reduce the number of bridging oxygen atoms in the Si-O bond and will decrease the fiber's viscosity. For example, water condensation reduces the fiber viscosity and may cause significant depolymerization [29].



So the HN-PCF should be pre-heated so as to reduce the condensation in the air holes.

In our experiment, because the propagation constant of the HN-PCF is less than that of the standard SMF, the SMF is pre-tapered with a pre-tapered length of 4mm in order to make its propagation constant close to that of HN-PCF. The pre-tapered SMF is twisted with the HN-PCF and put into the fiber holders. In order to remove the condensation in the air holes, the

hydrogen flow is increased from 30a.u. to 50.3a.u. at a speed of 2a.u./s. The hydrogen flow level of 50.3a.u. is the critical hydrogen flow level which makes the air-hole collapse speed equals to the taper speed in our experiment.

Figure 7 shows the power conversion in coupling process between SMF and HN-PCF based on the FBT technique. It can be seen that the coupling ratio is almost 90% at a taper length of 13mm. The coupling period decreases when the taper length increases, this is because the coupling coefficient gets larger when the taper length increases. The maximum coupling ratio fluctuates when the taper length increases. This is because the air-holes will collapse with stable hydrogen flow when the HN-PCF getting thinner. The burrs on the coupling curves are a result of the coupling between the fundamental mode of SMF and cladding modes of the HN-PCF.

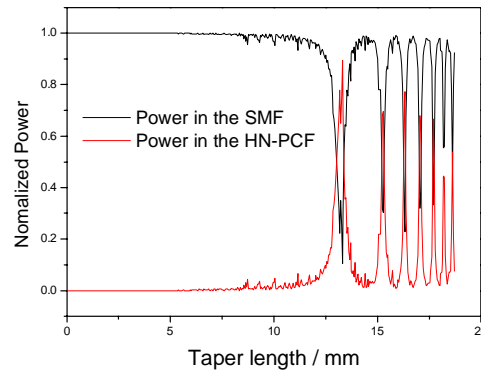


Fig. 7. The power transfer varies with the taper length in the coupling process between SMF and HN-PCF based on FBT technique.

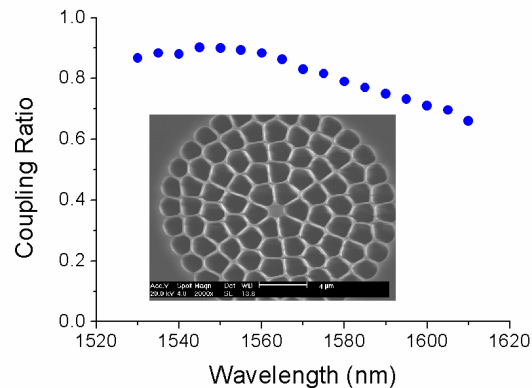


Fig. 8. The coupling ratio varies versus wavelength in the range of 1530~1610nm. The inset is the scanning electron microscope (SEM) images of the cross section of the fused PCF.

A SMF and HN-PCF coupler with coupler ratio of 90% at wavelength of 1550nm is achieved when the taper length is about 13mm. It can be seen from Fig.8 that coupling ratio will decrease when the wavelength deviates from 1550nm. The wavelength dependent property of the coupling ratio is due to the propagation constant varying versus the wavelength in the HN-PCF [1, 37]. As the waist of the fused PCF is so thin that its facet is very hard to be cleaved flatly, the cleaving point has been slightly off from the exact taper waist. The SEM image of the fused HN-PCF is shown in Fig. 8. Comparing the SEM image in

the Fig. 8 to that in the Fig. 4, it can be seen that the structure of the HN-PCF is well preserved in the coupling process.

4. Conclusions

To sum up, we propose that power can be transferred between a standard SMF and a HN-PCF by using the FBT technique instead of interface fusion splice. In our experiment, the SMF is pre-tapered to match its propagation constant to that of the HN-PCF. The twisted fiber is pre-heated before tapering to remove the condensation in the air-holes. Using an appropriate level of hydrogen flow to regulate the heating temperature is critical for preserving the HN-PCF's air holes to avoid collapse and softening the SMF. A coupling ratio of 90% is achieved in our experiment. The harmful Fresnel back-reflection, the large loss due to the MFD mismatch, nonalignment, air-hole collapse and bubble generation are avoided because of the FBT based coupling technique we use.

Acknowledgments

The authors would like to thank Dr. Huifeng Wei, Dr. Feng Tu, Dr. Honghai Wang of YOFC for providing the HN-PCF samples. The work is supported by Singapore A*STAR SERC project with Grant No. 0721010019.